JOURNAL OF GEOPHYSICAL RESEARCH, VOL. 113, C07005, doi:10.1029/2007JC004491, 2008

Mesoscale Atlantic water eddy off the Laptev Sea continental slope carries the signature of upstream interaction

I. A. Dmitrenko,[1] S. A. Kirillov,[2] V. V. Ivanov,[3] and R. A. Woodgate[4]

Received 9 August 2007; revised 12 February 2008; accepted 3 March 2008; published 2 July 2008.

[1] A mesoscale eddy formed by the interaction of inflows of Atlantic water (AW) from Fram Strait and the Barents Sea into the Arctic Ocean was observed in February 2005 off the Laptev Sea continental slope by a mooring equipped with a McLane Moored Profiler. The eddy was composed of two distinct, vertically aligned cores with a combined thickness of about 650 m. The upper core of approximately ambient density was warmer (2.6°C), saltier (34.88 psu), and vertically stably stratified. The lower core was cooler (0.1°C), fresher (34.81 psu), neutrally stratified and $\sim$0.02 kg/m^3 less dense than surrounding ambient water. The eddy, homogeneous out to a radius of at least 3.4 km, had a 14.5 km radius of maximum velocity, and an entire diameter of about 27 km. We hypothesize that the eddy was formed by the confluence of the Fram Strait and Barents Sea AW inflows into the Arctic Ocean that takes place north of the Kara Sea, about 1100 km upstream from the mooring location. The eddy's vertical structure is likely maintained by salt fingering and diffusive convection. The numerical simulation of one-dimensional thermal and salt diffusion equations reasonably reproduces the evolution of the eddy thermohaline patterns from the hypothesized source area to the mooring location, suggesting that the vertical processes of double-diffusive and shear instabilities may be more important than lateral processes for the evolution of the eddy. The eddy is able to carry its thermohaline anomaly several thousand kilometers downstream from its source location.

Citation: Dmitrenko, I. A., S. A. Kirillov, V. V. Ivanov, and R. A. Woodgate (2008), Mesoscale Atlantic water eddy off the Laptev Sea continental slope carries the signature of upstream interaction, *J. Geophys. Res.*, *113*, C07005, doi:10.1029/2007JC004491.

1. Introduction

[2] This paper discusses mooring observations, made off the Nansen Basin continental margin during February 2005, of an intermediate (80–700 m) depth eddy with two cores: an anomalously warm core in the upper part of the Atlantic water (AW) layer, and a cold core beneath. The presence of this remarkable feature has implications with respect to two important issues: lateral along-margin downstream transport of AW heat, and the double-diffusive modification of the lower AW layer. Previous studies suggest that an isolated eddy could travel thousands of kilometers through the Arctic Ocean over a period of several years and still retain the identity of its source water [*Newton et al.*, 1974; *Manley and Hunkins*, 1985; *D'Asaro*, 1988; *Muench et al.*, 2000]. Discrete eddies might transport their source waters far from their origin [*McWilliams*, 1985; *Kostianoy and Belkin*, 1989] and then inject those waters into the ocean interior by some decay process. The potential for eddies to shed salt and heat laterally into the ocean interior remains poorly known. The eddy decay process could be either gradual, by lateral intrusive or double diffusive processes, or catastrophic, by interaction with topography. In either case, the longevity of such isolated features has made eddies an ideal oceanic laboratory for the study of mixing processes [*Prater and Sanford*, 1994].

[3] The intermediate waters of the Arctic Ocean's Nansen Basin continental margins are influenced by the confluence of the warm and saline AW inflow through Fram Strait with the relatively colder and slightly fresher AW inflow through the Barents Sea that enters the Arctic Ocean between Franz Josef Land and Severnaya Zemlya (Figure 1). The difference in characteristics between the Fram Strait branch of AW (FSBW) and the Barents Sea branch of AW (BSBW) is mainly explained by the BSBW's air-sea interactions in the Barents Sea and the BSBW interaction with the fresher Norwegian Coastal Current [*Schauer et al.*, 2002a, 2002b]. The merged AW branches are found at intermediate (150–900 m) depths and follow the Eurasian Basin bathymetry in a cyclonic sense as a narrow, topographically trapped boundary current [*Timofeev*, 1957; *Aagaard*, 1989; *Woodgate et al.*, 2001; *Schauer at al.*, 2002b; *Karcher et al.*, 2003; *Polyakov et al.*, 2005; *Dmitrenko et al.*, 2008]. The cooler and slightly fresher BSBW is easily recognizable along the continental

[1]Department of Paleoceanography, Leibniz Institute of Marine Sciences, University of Kiel, Kiel, Germany.

[2]Department of Oceanology, Arctic and Antarctic Research Institute, St. Petersburg, Russia.

[3]International Arctic Research Center, University of Alaska Fairbanks, Fairbanks, Alaska, USA.

[4]Polar Science Center, Applied Physics Laboratory, University of Washington, Seattle, Washington, USA.

0148-0227/08/2007JC004491$09.00

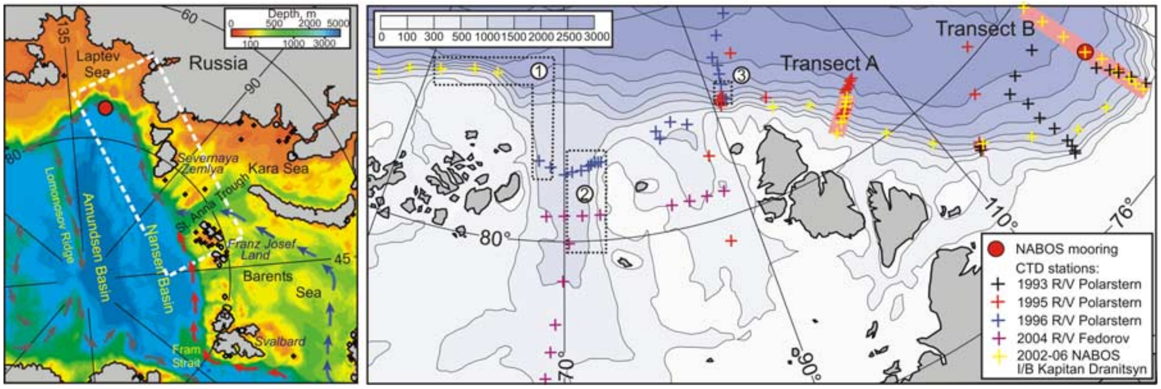

Figure 1. Map of the Arctic Ocean (left). Arrows trace the AW pathways; red and blue arrows show the Fram Strait and Barents Sea branches, respectively, of the AW inflow into the Arctic Ocean. The red circle marks the mooring position. The dashed rectangle encloses the Eurasian continental margin, which is enlarged in the right. Dotted lines enclose subregions upstream (subregions 1 and 2) and downstream (subregion 3) of the FSBW and BSBW confluence (right). Cross-slope transects A (September 2005 and 2006) and B (September 2002–2006) are shown by thick pink lines. Crosses mark the CTD stations occupied in August–September of 1993–2006. Bathymetry is adapted from the International Bathymetric Chart of the Arctic Ocean (IBCAO), 2001 version.

slope of the western Laptev Sea over the depth range of 400–1100 m downstream of the confluence with FSBW in the northern Kara Sea [*Schauer et al.*, 2002a, 2002b]. BSBW is also traceable in the Canada Basin [*McLaughlin et al.*, 2002; *Woodgate et al.*, 2007].

[4] During AW transit along the Eurasian Basin margins, the climatic mean FSBW core temperature decreases from 2.5–3.0°C near Svalbard down to 1.5°C along the western Laptev Sea continental margin [*Timofeev*, 1957; *Polyakov et al.*, 2003]; this decrease suggests that some fraction of the AW heat is lost during downstream propagation due to lateral and vertical heat exchange. One possible mechanism of AW transport is by way of eddies. However, detailed observations of eddies in the Arctic Ocean are scarce. Among previous reports of Arctic eddies [*Newton et al.*, 1974; *Manley and Hunkins*, 1985; *D'Asaro*, 1988; *Muench et al.*, 2000; *Woodgate et al.*, 2001] only the last one considers eddies in the Eurasian Basin. However, fixed-depth observations such as were made at several levels by *Woodgate et al.* [2001] are usually not sufficient to give an adequate eddy assessment.

[5] This paper describes a mesoscale eddy off the Laptev Sea continental slope for which daily vertical temperature, salinity, and velocity observations were obtained in February 2005 by a McLane Moored Profiler (MMP). The eddy clearly exhibits a unique structure consisting of two cores with distinct water properties: a warmer, saltier upper core and a colder, fresher lower core. This distinct eddy signature allows us to identify its source region, to assess its current state, and to hypothesize the mechanisms of eddy modification during translation from the source to the mooring position. The paper is structured as follows: section 2 is a brief description of data. Section 3 addresses several specific aspects of data processing that are important for further data interpretation. Section 4 describes the background oceanographic conditions (section 4.1) and the observed eddy features (section 4.2). Section 5.1 reveals the source area using the entire CTD (conductivity, temperature, and depth) data set available from upstream of the mooring position. The quantitative assessment of the eddy in section 5.2 employs the vertical density ratio and the gradient Richardson number to explore the system's susceptibility to double-diffusive and shear instabilities, respectively. In section 5.3 we examine the numerical solution of one-dimensional thermal and salt diffusion equations to reveal the main processes governing the modification of eddy thermohaline properties during eddy translation downstream from the source region. Section 6 summarizes our conclusions.

2. Data Set

[6] The data used in this study were collected from a mooring deployed at 78°26′N, 125°37′E offshore from the Laptev Sea continental slope (Figure 1). This mooring collected data during three consecutive years (2002–2003, 2003–2004, and 2004–2005); however, only the 2004–2005 data are employed for the present study. The mooring was equipped with an MMP, an instrument that samples an underwater vertical profile along a mooring line at a vertical speed of about 25 cm/s, with a sampling period of 0.5 s. The MMP is equipped with a CTD meter and an ACM (acoustic current meter), and records measurements of temperature, salinity, and velocity. The 2004–2005 deployment provided reliable CTD and current records between target depths of 80 and 900 dbar from 15 September 2004 until 20 February 2005. After that date, ballasting problems resulted in a gradual sinking of the MMP from the lower target depth of 900 dbar down to the bumper depth of 1880 dbar. The velocity record from the upward-looking Teledyne RD Instruments 300 kHz Workhorse Sentinel Acoustic Doppler Current Profiler (ADCP) installed at a depth of 54.5 dbar in 2004–2005 was employed for comparison with the upper-level MMP velocity record to verify the MMP's ACM velocity sensor measurements, as well as for tidal harmonic analysis.

[7] Mooring observations were complemented by oceanographic transects across the Laptev Sea continental slope (Figure 1, right) occupied during icebreaker *Kapitan*

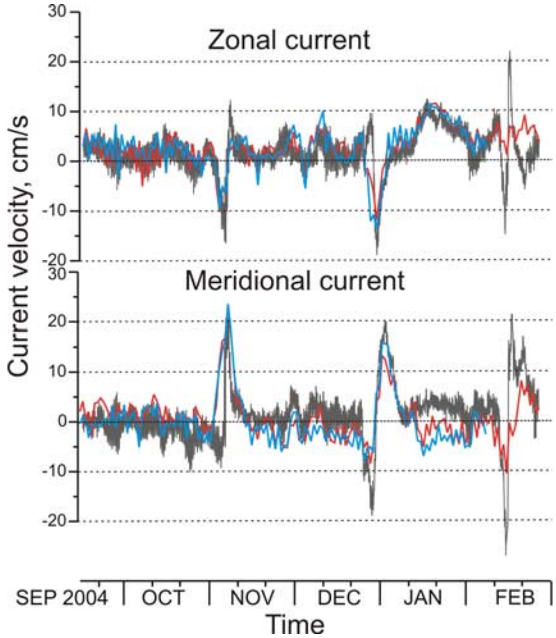

Figure 2. Zonal (top) and meridional (bottom) current velocity derived from the lower ADCP bin measurements at 48 dbar (gray), and 1 m binned uppermost MMP measurements made at 81 dbar (blue) and 100 dbar (red). The high-frequency oscillations of the ADCP-derived current velocity demonstrate magnitude of tidal currents.

Dranitsyn cruises in September 2005 and 2006 (transect A) and annually in September from 2002 to 2006 (transect B) using a shipboard Seabird SBE-19+ CTD and Lockheed Martin Sippican Expendable CTD (XCTDs–2006 only). In addition, the oceanographic transect along the Laptev Sea continental slope, approximately following the 1500 m depth contour, was carried out during icebreaker *Kapitan Dranitsyn* cruises in September 2005 (east of 95°E) and 2006 (31–64°E and east of 95°E) (Figure 1, right). These data were complemented by oceanographic stations occupied between 62°E and 126°E in August–September of 1993, 1995, 1996, and 2004 during the ARKIX-4 (1993), ARKXI-1 (1995), and ARKXII (1996) cruises of the RV *Polarstern* [*Schauer et al.*, 2002b] and the August–September 2004 cruise of the RV *Akademik Fedorov* (Figure 1, right).

[8] According to manufacturers' estimates, the individual temperature and conductivity measurements are accurate to ±0.005°C and ±0.0005 S/m, respectively, for the SBE-19+ (*Kapitan Dranitsyn*), ±0.001°C and ±0.0003 S/m for the SBE-911 (*Akademik Fedorov*), and ±0.003°C and 0.0005 S/m for the modified Neil Brown Mark III b (*Polarstern*). XBT temperature and conductivity sensors are accurate to ±0.02°C and ±0.003 S/m, respectively. At the mooring, the MMP carried an SBE 41CP CTD sensor with temperature, conductivity, and depth measurement accuracies of ±0.002°C, ±0.0002 S/m, and ±2.4 dbars, respectively. The precision and resolution of current velocity measurements made by the MMP's Falmouth Scientific, Inc. (FSI) ACM are reported by FSI to be ±2% of reading, or 1 cm/s and ±0.01 cm/s, respectively. Compass accuracy is ±2°. ADCP precision and resolution are reported to be ±0.5% of reading and ±0.1 cm/s, respectively. Compass accuracy is ±5°. The ADCP operated at 307.2 KHz frequency with 4 m depth cell size, 2 Hz ping rate, 30 min ensemble time interval, and 30 pings per ensemble. The BroadBand mode single-ping standard deviation for the 4 m depth cell size is reported by Teledyne RD Instruments to be 3 cm/s.

3. Data Processing

[9] There are two issues we raise in this section. The first issue is related to correction of the MMP conductivity sensor thermal mass error using an algorithm reported by *Johnson et al.* [2007]. The second issue deals with the upward-looking ADCP data that we employ to verify the MMP velocity record and to estimate the range of tidal currents.

[10] Salinity reported immediately after the MMP has crossed a strong thermal gradient can be in error as a result of the conductivity cell's thermal mass. This error arises because of heat exchange between the conductivity cell and the water within it [*Johnson et al.*, 2007]. During the MMP profiling, particularly through the center of an eddy, the MMP has transited through the several diffusive thermohaline staircases observed at the interface between the upper and lower eddy cores (see section 4.2 for more details). Salinity, measured through the vertical temperature gradient of about 0.08°C/m from warm to cold water of the thermohaline staircases, exhibits an error exceeding 0.013 psu, resulting in unstable saltier spikes of about 0.02 kg/m^3 in potential density at the base of the mixed layers (not shown).

[11] The MMP is equipped with a SBE-41 CP CTD. The detailed SBE-41 CP CTD sensor response correction has been recently quantified by *Johnson et al.* [2007]. We employed their algorithm to correct the MMP vertical profiles of salinity and density. All parameters that vary the amplitude and time-scale of the conductivity cell's thermal mass correction and minimize the variation within the constant-temperature portion of the thermohaline staircase itself were derived from the algorithm described by *Johnson et al.* [2007].

[12] In addition to the conductivity cell's thermal mass error, the short time-scale (point-to-point) salinity spikes are found while and just after the instrument moves through strong temperature gradients. These spikes arise because of short time-scale mismatches between the temperature and conductivity cells. By varying the parameter responsible for these spike corrections we can match the temperature and conductivity response time. In fact, correction parameters may vary from one CTD sensor to another. In our case we found that the zero setting tends to minimize the short time-scale salinity spikes, suggesting that the temperature and conductivity response times are pretty well matched [G. C. Johnson, personal communication, 2007].

[13] The upward-looking ADCP current record measuring through the depth range of 5–48.5 dbar was employed, first to verify the MMP velocimeter record, and second to determine to what extent tidal currents may disrupt the eddy velocity signature. The high-quality MMP velocimeter record is confirmed by reasonable agreement between the uppermost MMP measurements at 81 dbar and the lower ADCP bin taken at 48.5 dbar (Figure 2).

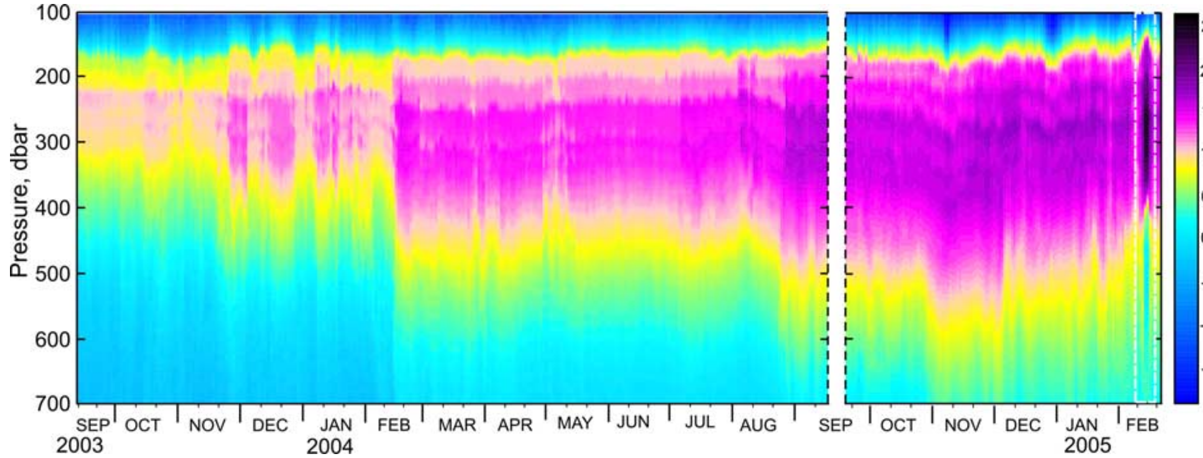

Figure 3. Water temperature (°C) from the McLane Moored Profiler (MMP). The dashed vertical rectangle (February 2005) indicates the transformation of water temperature by the passing eddy. The gap in September 2004 represents redeployment.

[14] Our data suggest that tidal currents are too small to interfere with the eddy velocity signature. The tidal currents for the main tidal harmonics were estimated from the ADCP velocity record using an algorithm by *Foreman* [1977] for the 20–48.5 m water layer. To avoid the underestimation of tidal currents due to interaction with the boundary layer beneath the ice, we do not include the ADCP data from the upper bins between 5 and 20 m in this analysis. Monthly amplitudes of the main tidal harmonics were computed for all bins throughout the entire duration of the ADCP record with a time lag of 24 h. Afterward, these amplitudes were averaged vertically and through the period of observations from September 2004 to February 2005. Our tidal analysis revealed the predominance of lunar semidiurnal tidal currents with amplitude of 1.7 cm/s. In fact, the tidal current composed of all tidal components does not exceed 4–5 cm/s, as is well illustrated by the high-frequency tidal oscillations of the ADCP-derived current velocity shown in Figure 2. Figure 2 also illustrates that for all three eddies captured by the mooring in the beginning of November, end of December, and middle of February, the tidal current of about 25–30% of the eddy swirl velocity does not appear to interfere with the eddy velocity signature (Figure 2). Particularly, for the eddy event of February 2005 (the focus of this paper), the tidal-current amplitude of about 3 cm/s is substantially less than the eddy's tangential velocity of 9–13 cm/s (Figure 2; see also section 4.2 for more details). Thus we assume that the eddy velocity signature is not substantially affected by tides. A tidal signal of negligible amplitude remains in the MMP velocity record used for calculating the gradient Richardson number in section 5.2.

4. Results

4.1. Background Atlantic Water Oceanography

[15] Over the past several decades the FSBW has exhibited substantial variability. Shifts in atmospheric circulation patterns have resulted in increased transport and temperature of AW entering the Arctic via Fram Strait [*Rudels et al.*, 2000]. The first evidence of strong warming within the FSBW layer was found in the Nansen Basin in 1990 [*Quadfasel et al.*, 1991]. Positive AW anomalies of up to 1°C were carried along the continental margins into the Arctic Ocean interior [*Carmack et al.*, 1995; *Woodgate et al.*, 2001; *Schauer et al.*, 2002b]. *Polyakov et al.* [2004] found that the 1990s maximum fits well with a recurring pattern of multidecadal AW variability that occurs over a timescale of 50–80 years. Since the late 1990s, AW temperature has shown a new tendency to increase [*Schauer et al.*, 2004; *Polyakov et al.*, 2005; *Dmitrenko et al.*, 2008]. While the FSBW continuous warming of the 2000s is well documented over the Siberian margin, the tendency of the BSBW remains poorly known. Recently *Rozkhova et al.* [2008] reported a contrary tendency of the BSBW to cool due to its longer residence time over the eastern Barents Sea. The BSBW cooling from the beginning of the 2000s was also reported by *Woodgate et al.* [2007].

[16] Our one-and-a-half-year-long MMP temperature record from the mooring also exhibits substantial AW layer temporal variability (Figure 3). Before February 2004 this variability is consistent with a seasonal cycle, with AW winter temperatures generally higher than summer temperatures (Figure 3). This variability is generated by the wind-driven seasonal shift of the AW jet toward the slope in winter and away from the slope in summer [*Dmitrenko et al.*, 2006]. After February 2004 this seasonal pattern was disrupted by a warming event that can be clearly seen in the MMP record (Figure 3), when the MMP captured an exceptionally strong warming with an AW temperature increase of about 0.4°C. This warming event has been attributed to downstream propagation of the AW warm anomaly first recorded in the Fram Strait in 1999 [*Schauer et al.*, 2004; *Polyakov et al.*, 2005]. A second AW temperature increase of about the same magnitude was captured in August 2004 measurements (Figure 3). After August 2004 a continuous gradual temperature increase that continued until November 2004 was accompanied by AW layer thickening, and deepening of the AW core by 55 m. From November 2004 until the end of the observational period in February 2005, when the eddy was captured (Figures 3 and 4), the AW layer gradually returned to the conditions of September 2004.

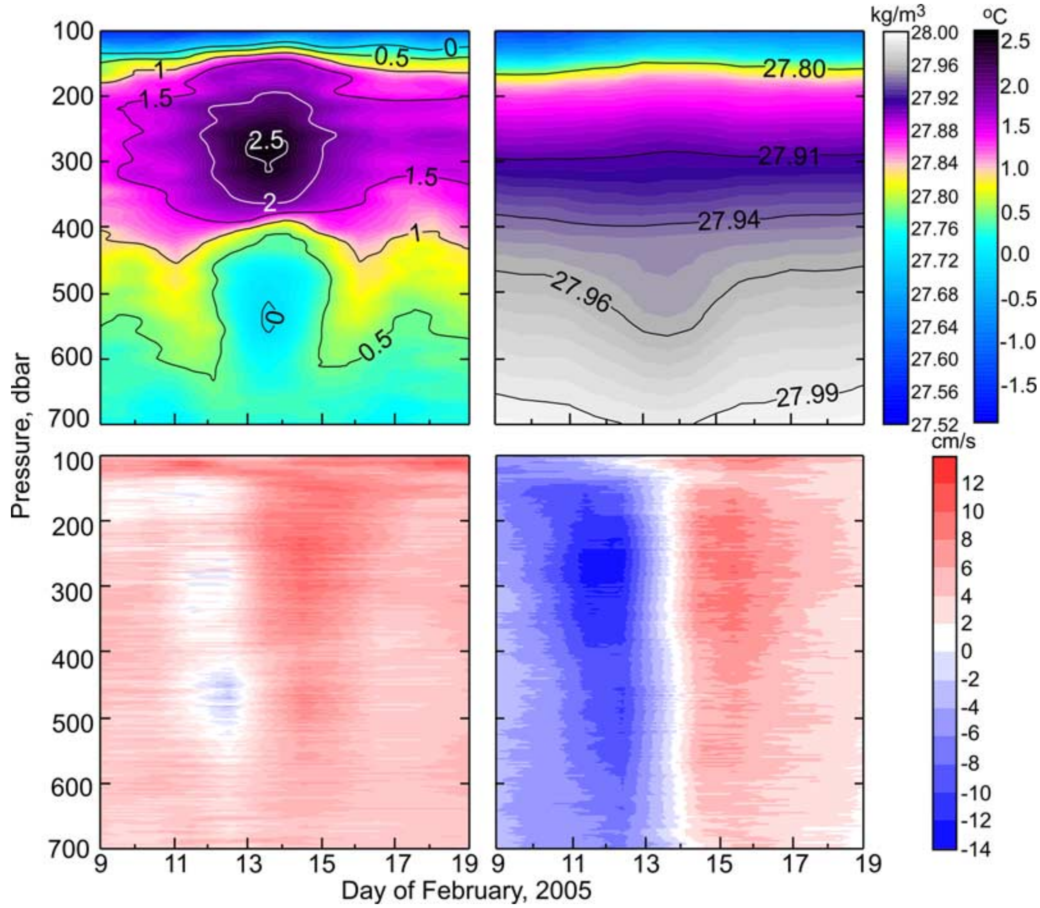

Figure 4. An enlarged view of the February 2005 eddy. Temperature (°C, top left), potential density (kg/m^3, top right), and zonal (bottom left) and meridional (bottom right) current (cm/s) records as a function of depth; McLane Moored Profiler (MMP) records from 9–19 February 2005.

[17] The 5-month mean (September 2004 to February 2005) MMP-derived temperature-salinity (T-S) plot (Figure 5, top left) did not clearly exhibit the T-S intermediate minima beneath the FSBW that would indicate the presence of the BSBW. This is consistent with the findings of *Schauer et al.* [1997] from the period of the AW warming of the 1990s that over the Laptev Sea continental slope the FSBW and the BSBW have already lost much of their original thermohaline properties through mixing. Note, however, that the BSBW has later proved to be traceable in the Canada Basin [*McLaughlin et al.*, 2002]. *Woodgate et al.* [2007] also traced the BSBW in the Canada Basin during both a warmer AW phase of the 1990s and a cooler AW phase from the beginning of the 2000s.

4.2. Observed Features

[18] From 10–18 February 2005 the MMP captured an eddy with anomalous temperature and salinity characteristics (Figure 3, area marked by dashed vertical rectangle, and Figures 4 and 6). Vertical temperature profiles taken on 13–14 February 2005 through the eddy center reveal two different anomalous properties: a warmer and saltier core in the upper AW layer (100–390 m) and a cooler and fresher core in the lower AW layer (390–650 m) (Figure 4, top left, and Figure 6). The vertical gradients of temperature and salinity through the interface between the upper and lower cores were 0.011°C/m and 8.33 10^{-4} psu/m, respectively.

[19] The highest core temperature of 2.6°C occurred at about 280 m on 13–14 February 2005, exceeding the temperature in the surrounding ambient water by about 1°C (Figure 4, top left, and Figure 6, left). The eddy's warm core temperature also exceeds the 5-month mean AW core temperature by about five standard deviations (Figure 5, top left). Furthermore, the eddy's warm core temperature exceeds the absolute maximum AW temperature recorded over the entire period of CTD observations in this area (1993–2006) by 0.04°C. The coldest core temperature occurred between about 490 and 550 m, where temperature ranged from 0.7°C in the ambient waters (10 and 17 February 2005) to 0.1°C in the eddy core (13–14 February 2005) (Figure 4, top left and Figure 6, left). As for the upper core, the lower core negative temperature anomaly exceeded the 5-month mean temperature at the same potential density level by about 5 standard deviations (Figure 5, top left). Salinity within the warm core was higher than ambient by 0.1 psu, while the cold core salinity was 0.07 psu lower than ambient (Figure 6, center). The temperature and salinity eddy signatures were not discernable deeper than about 660 m (Figure 6). Closer to the surface, recognition of the temperature and salinity anomalies was limited by the upper target depth of MMP

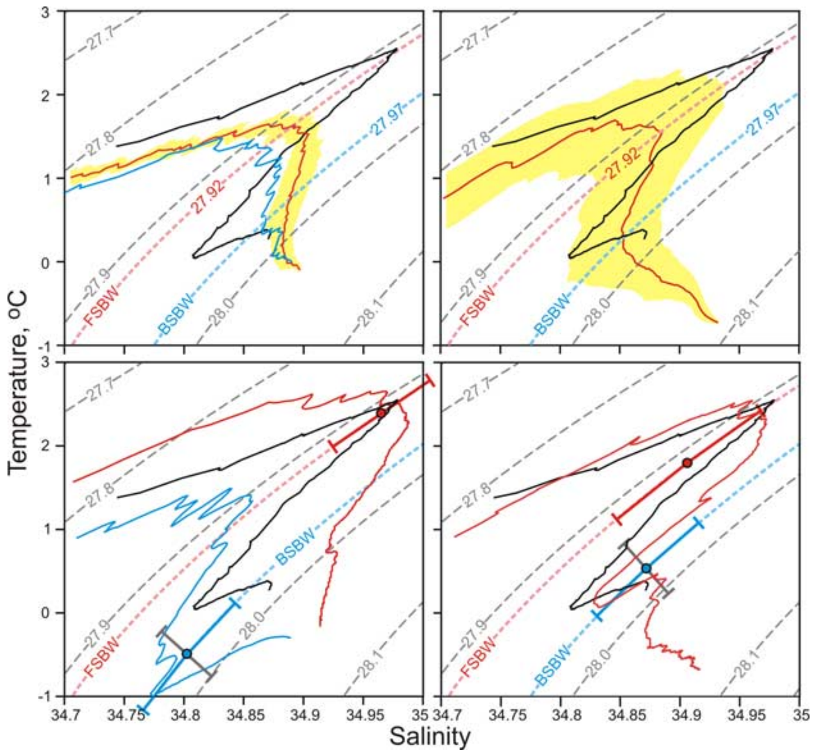

Figure 5. The black line shows the T-S diagram for the MMP CTD cast taken through the eddy center on 14 February 2005, and dashed lines are isopycnals referenced to the sea surface in kg/m^3: Pink and blue dashed lines identify the mean potential density of the FSBW and BSBW, respectively. (top left) The T-S diagram of profiles taken through the eddy center on 14 February 2005 (black), and in the ambient water on 9 February 2005 (blue). The T-S diagram for the 5-month mean profile (September 2004 to February 2005), obtained by averaging along potential isopycnals, is shown by the red line. (top right) The red line shows a T-S diagram of the mean of all shipboard CTD profiles taken between 90°E and 120°E from 1993 to 2006 which exhibit the BSBW signature. (top) The yellow shading indicates ±one standard deviation of the mean. (bottom left) The blue and red lines are T-S diagrams for typical CTD profiles taken through the BSBW core (blue: subregion 2, expedition ARKXII, July 1996, 81.262°N, 70.945°E) and the FSBW core (red: subregion 1, expedition NABOS, September 2006, 83.032°N 59.936°E) upstream of their confluence in the northern Kara Sea. (bottom right) The red line is the T-S diagram of the typical CTD profile taken through the FSBW and BSBW cores downstream of their confluence in the northern Kara Sea (subregion 3, expedition ARKXI-1, September 1995, 82.140°N, 91.404°E). (bottom) Dots show mean T-S characteristics and along-isopycnal error bars show ±one standard deviation in the core of the FSBW (red: 27.92 ± 0.01 kg/m^3) and the BSBW (blue: 27.97 ± 0.01 kg/m^3) over subregions 1 and 2 (left), and subregion 3 (right; see Figure 1 for subregions); black cross-isopycnal error bars indicate ± one standard deviation of the mean BSBW potential density.

observations (80 m), but the ADCP velocity observations also captured the eddy in the upper water layer (Figure 2).

[20] The density stratification is not uniform throughout the upper and lower cores. The upper core consists of stably stratified layers. The upper core potential density is about 27.918 kg/m^3 (Figure 4, top right, and Figure 6, right), not very different from the ambient water, and similar to the 27.92 kg/m^3 mean potential density of the AW core obtained by averaging temperature and salinity along the potential isopycnals through all CTD profiles taken over the Eurasian continental margin between 90°E and 120°E (Figure 5, top right). The 27.95 kg/m^3 potential density of the lower core was 0.02 kg/m^3 lower than ambient (Figure 5, top left, and Figure 6, right). While the upper core is stably stratified by density, the lower core is neutrally stratified from about 425–555 m (Figure 6, right). Of particular interest is that the lower part of this layer, from about 475 m to 555 m, is completely mixed and the upper part, from about 425 m to 475 m, is neutrally stratified by density, while temperature and salinity decrease with depth (Figure 6).

[21] The eddy structure exhibits both temperature and salinity anomalies relative to the ambient surrounding waters for both upper and lower cores (Figure 6, two left panels). However, eddy baroclinicity is mainly attributed only to the negative density anomaly in the lower core layer (Figure 4, top right, Figure 5, top left, and Figure 6, right).

[22] Vertical profiles of zonal and meridional current speed, measured by MMP ACM, are shown in Figure 4 (bottom). Anticyclonic circulation is evident in both cores. Moreover, both cores are recognizable by their maximum tangential speeds. The greatest tangential speed, exceeding

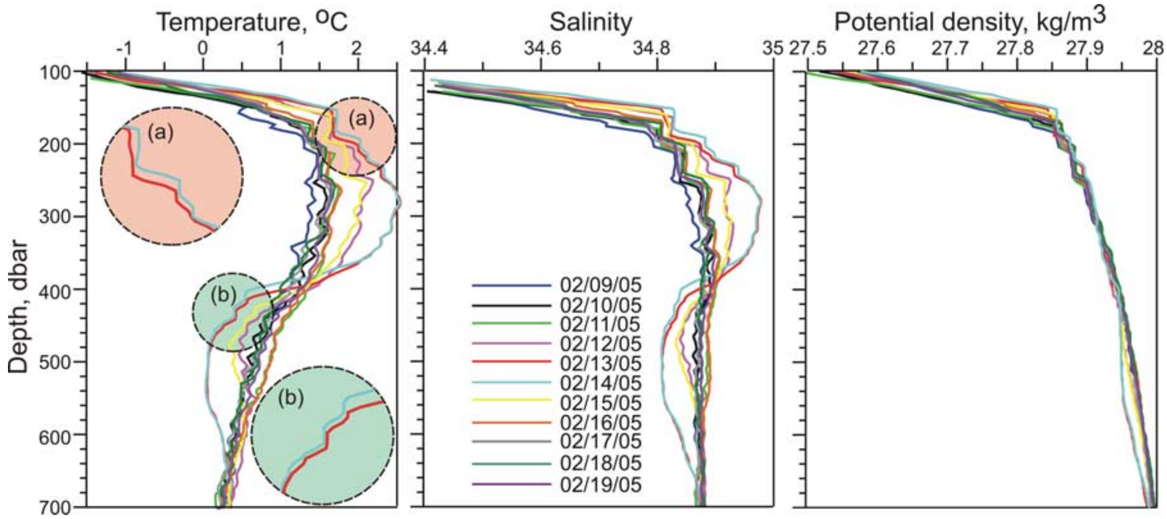

Figure 6. Vertical profiles of temperature (left), salinity (center), and potential density (right) taken by moored MMP CTD from 9–19 February 2005 as a function of depth. The enlarged views on the left show (a) diffusive and (b) salt-fingering interfaces through the eddy center.

13 cm/s, marks the center of the upper core near 280 m depth. This depth coincides with the depth of the greatest temperature and salinity anomalies. Almost the entire upper core exhibits a fairly vertically uniform tangential speed of 12 cm/s. The tangential speed of the lower core does not exceed 9 cm/s; the velocity signature of the lower core is much weaker, and recognizable only in the 450–510 m layer (Figure 4, bottom). The velocity signature of the entire eddy is not discernable deeper than about 700 m, where the tangential speed of 2–3 cm/s is close to the 1 cm/s ACM sensor accuracy. This depth approximately coincides with the lower depth at which temperature and salinity anomalies vanish in the eddy center. The upward-looking ADCP velocity record identifies the upper eddy depth at 21 m (not shown).

[23] The length scale of the eddy was estimated from the duration of the event and the average flow velocity. The four-day duration was defined as occurring between the dates of highest tangential current speed (12 February and 16 February 2005), and the 4.3 cm/s velocity was obtained by averaging throughout the water depth range of 100–690 m between these dates. The eddy radius, defined as the distance from the approximate center to the point of highest tangential current speed, was 7.4 km. The entire diameter of 27 km corresponds to the entire duration of the event, defined as the entire period during which the eddy's velocity signature can be recognized (10–18 February 2005); the flow velocity averaged over that time period is 3.9 cm/s. This spatial structure corresponds well to that reported by *Newton et al.* [1974] for the eddy observed during the Arctic Ice Dynamics Joint Experiment in the Canada Basin. It also roughly agrees with the internal Rossby radius of deformation of about 10 km. Note that due to uncertainty of mooring position relative to the eddy trajectory, the eddy length scale shown above represents the lower bound.

[24] Comparison of the mean flow during the eddy event (velocity and direction of 3.9 cm/s and 83°, respectively, from 10–18 February 2005) with a background monthly mean (velocity and direction of 5.7 cm/s and 81°, respectively, from January–February 2005) did not reveal substantial difference. These mean flow estimations are consistent with those reported by *Woodgate et al.* [2001] at ~5 cm/s from the 1995–1996 mooring velocity and TS advection data near the junction of the Lomonosov Ridge with the Eurasian continent. Note that *Dmitrenko et al.* [2008] estimated the lower mean flow at ~2.4 cm/s downstream from the mooring site based on 2003–2005 data from moored current meters and TS advection data from the along-slope CTD survey of 2005.

[25] The other two eddies captured by the moored ADCP (Figure 2) and the MMP (Figure 3, right) in the beginning of November and the end of December exhibit a cooler and fresher core located in the cold halocline overlying the AW layer (see right panel in Figure 3 for temperature distribution). *Woodgate et al.* [2001] suggest that such eddies can be generated in the Laptev Sea winter coastal polynyas from the cold and saltier water plumes produced episodically at polynya openings due to brine release at polynya ice formation. Although the water in the polynya is more saline than the surrounding shelf waters, the polynya water is fresher than waters of the same density over the slope [*Woodgate et al.*, 2001].

5. Discussion

5.1. Source Region

[26] As previously indicated, the eddy displayed T-S characteristics which differ from those of the ambient water, implying that it was created at another location where different temperature and salinity characteristics prevail. We argue that the upstream observations (see Figure 1, right for observation locations) provide evidence that the warmer and saltier upper core water originates from the upstream FSBW, and the colder and fresher deeper core is attributed to the upstream BSBW.

[27] First, we compare the potential density of the upper and lower eddy cores with the mean densities of the FSBW and the BSBW downstream of their confluence in the

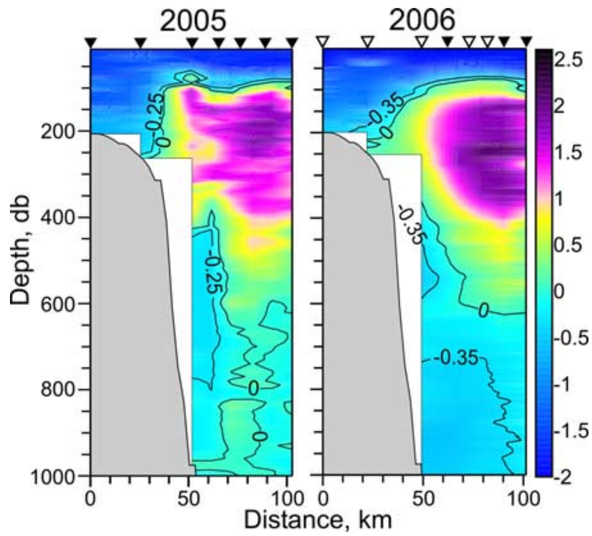

Figure 7. 10-m binned temperature (°C) sections A taken in September 2005 (left) and 2006 (right) across the western Laptev Sea continental slope. Black and white arrows on the top show the CTD and XCTD stations, respectively.

northern Kara Sea. The mean vertical profiles of temperature and salinity were computed by averaging the individual CTD profiles measured off the continental shelf break between 90°E and 120°E in 1993–2006 (Figure 1). In this area the BSBW jet is relatively narrow cross-slope, and usually is found shifted on-slope, while the FSBW jet is shifted more off-slope [for example see *Schauer et al.*, 2002b]. The temperature cross-slope section A (see right panel in Figure 1 for section position) taken in September 2005 and 2006 is consistent with this regular pattern (Figure 7). CTD profiles taken over the lower continental slope usually do not exhibit the BSBW signature. Note that for the mean computation only T-S profiles with the BSBW signature were taken into account. Temperature and salinity profiles were averaged over the potential isopycnals. The T-S diagram for this spatially averaged profile reveals a mean potential density for the FSBW of about 27.92 kg/m^3 (Figure 5, top right). The BSBW exhibits a mean potential density of about 27.97 kg/m^3. While the density of the eddy's upper core corresponds well to the FSBW mean, the lower core density differs from the BSBW mean by about 0.02 kg/m^3 (Figure 5, top right).

[28] Second, we demonstrate that the T-S characteristics and potential density for the upper and lower cores agree reasonably well with characteristics and potential density measured in representative individual CTD profiles, taken from subregions 1 and 2 upstream of the FSBW and BSBW confluence (Figure 1, right). The statistical representation of these profiles is confirmed by reasonable agreement of the FSBW and the BSBW core characteristics with subregional mean values, shown by dots with error bars in Figure 5 (bottom). The along-isopycnal error bars show the temperature and salinity standard deviations over the range of ±0.01 kg/m^3 relative to the FSBW and BSBW mean potential densities. The cross-isopycnal error bars demonstrate the potential density standard deviations for the BSBW core.

[29] Northeast of Franz Josef Land the FSBW, following the bathymetry, splits into two branches; one flows further east along the continental slope, and the other enters the northern Kara Sea along the western flank of the St. Anna Trough [*Hanzlick and Aagaard*, 1980; *Schauer et al.*, 2002a] (subregion 1 in Figure 1, right). The FSBW core characteristics were derived from the CTD profile, taken in September 2006 off-slope near Franz Josef Land at 83.032°N 59.936°E at about 2000 m water depth (Figure 1, right). Those characteristics are in excellent agreement with mean FSBW core T-S characteristics from subregion 1, and the eddy upper core data (Figure 5, bottom left). This close agreement suggests that there was no substantial exchange between the upper eddy core and the ambient water during the eddy's along-slope translation from the northern Kara Sea to the northern Laptev Sea.

[30] Outflow of the BSBW to the Eurasian Basin occurs along the eastern flank of the St. Anna Trough [*Schauer et al.*, 2002a] (subregion 2 in Figure 1, right). The BSBW core characteristics were derived from the representative CTD profile taken in July 1996 at the eastern flank of the St. Anna Trough at 81.262°N, 70.945°E (Figure 1, right). While the BSBW core temperature and salinity measured at the St. Anna Trough are lower than the mean of all measurements from subregion 2, the potential density is consistent (Figure 5, bottom left). The lower eddy core temperature of 0.1°C is warmer than both the BSBW mean from subregion 2, and the BSBW from the 1996 CTD profile by 0.5°C and 1.1°C, respectively. While the potential density of the lower eddy core is 0.02 kg/m^3 lower than the subregional mean, it is still within the range of one standard deviation (Figure 5, bottom left).

[31] Focus upon the probable source of the eddy also requires consideration of possible generation mechanisms. *Woodgate et al.* [2001] suggested that eddies extending to depths of more than 1000 m observed near the junction of the Lomonosov Ridge with the Eurasian continental margin (Figure 1, left) originate from an instability in the front that forms between the FSBW and the BSBW in or near the St. Anna Trough. Near the formation region the front is sharpest and most unstable, but downstream, horizontal mixing between the FSBW and the BSBW erodes the front, leaving no clear horizontal distinction between the two branches [*Woodgate et al.*, 2001]. *Schauer et al.* [1997] showed that downstream of the confluence between the FSBW and the BSBW, the boundary AW current can be baroclinically unstable. Furthermore, they argued that inflow of the BSBW may provide an additional destabilizing effect for the FSBW. *Schauer et al.* [2002b] demonstrated that the density distribution at several off-slope stations north of the Severnaya Zemlya is consistent with a subsurface anticyclonic baroclinic eddy field. They also reported several deeper water lenses that were colder and lower in salinity, presumably formed from cross-frontal interaction between the BSBW and the water beneath the FSBW core.

[32] While there is no direct evidence of an unstable vertical interface between the FSBW and the BSBW, the CTD profiles taken at the vicinity of the suggested front are similar to those taken through the eddy core 1111 km downstream along-slope. The BSBW and that part of the FSBW which had not entered the St. Anna Trough are clearly evident in the water mass properties in the Eurasian

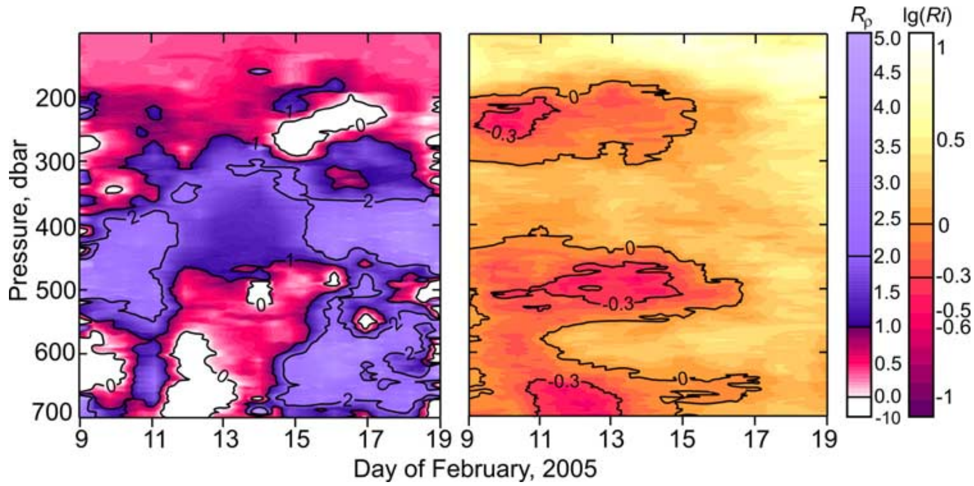

Figure 8. Vertical density ratio R_ρ (left) and the gradient Richardson number Ri (right, logarithmic scale) calculated through the eddy as a function of depth show the system's susceptibility to double-diffusive and shear instability, respectively. Note that the shear instability may occur at lg (Ri) < 0. The salt-finger convection occurs when $R_\rho > 1$, and the diffusive convection occurs when $0 < R_\rho < 1$. Stable conditions are characterized by $R_\rho < 0$.

Basin north of the Kara Sea [*Schauer et al.*, 2002b] (subregion 3 in Figure 1, right). The 1996 cross-slope section reveals the narrow (30 km wide) BSBW, cool and less saline, tracked on-slope to a depth of 1800 m beneath the off-slope-shifted FSBW [see *Schauer et al.*, 2002b, Figure 5]. Since both cores were relatively narrow cross-slope, their mean T-S characteristics, obtained through the cross-slope extended subregion 3 (Figure 1, right), differ from the characteristics of the individual CTD profile, taken on September 1995 at 82.140°N, 91.404°E (Figure 5, bottom right); however the FSBW and the BSBW core characteristics for this particular profile fall within the range of one standard deviation of the mean (Figure 5, bottom right). Moreover, the T-S structure of this individual, but representative, profile resembles closely with the T-S structure of the eddy core (Figure 5, bottom right). The density difference of about 0.015 kg/m^3 between the BSBW core and the lower eddy core is within the range of one standard deviation of the subregional mean. The increase in BSBW temperature (by about 1.0°C) and salinity (by about 0.05 psu) during transition along the western flank of the St. Anna Trough to the confluence with the FSBW are also evident through comparison of core characteristics derived from both the individual profiles and the subregional mean (Figure 5, bottom panels). This transformation of thermohaline properties can be attributed to mixing of the BSBW with the FSBW recirculating along the St. Anna Trough.

5.2 Quantitative Assessment of the Eddy's State

[33] The FSBW enters the Arctic Ocean as a warmer and saltier intermediate layer, forming the vertical stratification that is favorable for double-diffusive mixing over the entire Arctic Ocean [*Rudels et al.*, 1999; *Merryfield*, 2002]. The confluence between the FSBW and BSBW cores in the northern Kara Sea results in conditions unstable with respect to salt fingering at the sharper interface between the warmer and saltier FSBW above and the cooler and fresher BSBW below; furthermore, this instability creates the preconditions required to allow diffusive convection through the interface between the BSBW and warmer and saltier ambient water beneath. In this section we will show that the vertical temperature and salinity distribution in the eddy core is conditioned by diffusive convection which transports temperature more effectively than salt above the FSBW core and beneath the BSBW core, and salt fingering convection, which transports salt more effectively than heat through the interface between the FSBW and the BSBW cores.

[34] The double-diffusive activity is parameterized by the vertical density ratio which is defined as $R_\rho = \alpha T_z/\beta S_z$ [*Turner*, 1973], where $\alpha = (1/\rho)(\partial\rho/\partial T)$ is the thermal expansion coefficient, $\beta = (1/\rho)(\partial\rho/\partial S)$ is the haline contraction coefficient, and T_z and S_z are the local vertical gradients of temperature and salinity, respectively. The density ratio is the ratio of change in density due to temperature to change in density due to salinity. On the basis of results from theory, laboratory experiments, and oceanic observations, the vertical density ratio is believed to be a useful indicator of double-diffusive stability [*Ruddick*, 1983]. The density ratios are conducive to both salt fingering ($R_\rho > 1$) and diffusive ($0 < R_\rho < 1$) types of double-diffusive mixing, as is typical for many density-compensated, vertical interfaces along which interleaving occurs. We analyze physical properties of the eddy water using the density ratio as an index of susceptibility to the double-diffusive convection.

[35] The relative influence of temperature and salinity on vertical density stratification through the eddy is presented in Figure 8, left. The distribution of R_ρ identifies several sublayers that are stably stratified by density, but favors the double-diffusive instability. The diffusive convection occurs in the upper layer of the FSBW core where colder, fresher water overlays warmer, saline water. The stable salinity

stratification overcompensates for unstable temperature stratification, and the water remains stably stratified by density. This regime is characterized by a density ratio that varies from 0 to 1 (red color in Figure 8, left). Salt fingering convection occurs across the interface between the FSBW and the BSBW eddy cores, where warmer and saline FSBW overlays the cooler and fresher BSBW. The stable temperature stratification overcompensates for the unstable salinity stratification and the water remains stably stratified in density. This regime is characterized by a density ratio exceeding 1 (violet color in Figure 8, left).

[36] The vertical patterns described above are the intrinsic features of the vast area downstream of the FSBW and the BSBW confluence in the northern Kara Sea. However, the vertical thermohaline structure of the measured eddy shows one more feature that is different from the surrounding waters. Except for the higher temperature and salinity gradients between warm and cold eddy cores at depths of 350–400 m, the cold BSBW forms an embedded maximum in temperature at about 650 m (Figure 6, left), resulting in the appearance of one more region favorable for diffusive convection at depths of 550–650 m. Ambient waters do not exhibit this feature due to the intensive thermal modification of colder BSBW after its confluence with the FSBW in the northern Kara sea (see also Figure 5, top).

[37] There is evidence indicating that double diffusion is important in controlling the diapycnal mixing process in the ocean only if R_ρ is sufficiently close to 1. *Schmitt* [1981] reviews several investigations that show a consistent decrease in salt-finger activity with increasing R_ρ. At density ratios above 2, salt-fingering activity seems to be very low. *Zhang et al.* [1998] suggested that a density ratio interval of $0.33 < R_\rho < 0.77$ and $0.77 < R_\rho < 1$ would be appropriate for moderate and strong diffusive convection mixing rates, respectively. Note that the regions of enhanced double-diffusive mixing (with $0.5 < R_\rho < 2$) occupy the entire 200–500 m layer through the eddy center (13–14 February, Figure 8, left).

[38] The gradient Richardson number provides a strong constraint for identifying turbulence produced by shear instability. It is defined as:

$$Ri = \frac{N^2}{S^2}, \tag{1}$$

where N is Brunt-Vaisala frequency, and $S^2 = U_z^2 + V_z^2$ is squared vertical shear of flow. According to the inviscid theory of *Miles* [1961, 1963] and *Howard* [1961] the flow should be stable and laminar if $Ri > 0.25$. While $Ri < 0.25$ is the generally accepted critical value below which turbulence can be expected, in fact, turbulent mixing can and does occur at higher values of $Ri < 1$ [*Abarbanel et al.*, 1984; *Miles*, 1986; *Polzin*, 1996].

[39] The MMP velocity record through the eddy was used to compute the gradient Richardson number with the aim of evaluating flow stability. As seen in Figure 8 (right), and based on the usual criterion for shear instability of $Ri < 0.25$, there is no evidence of shear that is sufficient to transfer the background stratification into the mixed layer. However, Richardson numbers less than 0.5 are evident in the lower BSBW core and through the eddy front at its upper and lower boundaries (Figure 8, right). However, a general increase of turbulent dissipation at $Ri < 1$ as observed by *Polzin* [1996] assumes background turbulent diffusivity through almost the entire eddy (Figure 8, right).

[40] Below we reveal the relative contribution to eddy thermohaline structure formation of heat and salt exchanges due to salt-fingering and diffusive convection. We employ several well-known parameterizations of double-diffusive mixing. For the salt fingering we apply a parameterization by *Schmitt* [1981]:

$$K_T = \frac{0.7 \cdot K_*}{R_\rho \cdot \left(1 + \left(R_\rho / R_c\right)^n\right)} \tag{2}$$

$$K_S = \frac{K_*}{\left(1 + \left(R_\rho / R_c\right)^n\right)}, \tag{3}$$

where K_S and K_T are the diapycnal eddy diffusivities for salinity and temperature, respectively; K_* is the maximum diapycnal diffusivity due to salt fingering; R_c is the critical density ratio above which the diapycnal salt fingering mixing drops dramatically due to the absence of staircases ($R_c = 1.6$); and n is an empirical constant ($n = 6$). After *Zhang et al.* [1998] we have chosen a more modest value for the K_* (10^{-4} m^2/s) than originally proposed by *Schmitt* [1981], reflecting the fluxes in thermohaline staircases observed in the Caribbean Sheets and Layers Transects program [*Schmitt*, 1988; *Schmitt et al.*, 2005].

[41] *Kelley* [1984, 1990] suggested a parameterization for diffusive convection in which the laboratory-derived double-diffusive flux laws were applied to a set of oceanic data. The formulation was given as follows:

$$K_T = C \cdot f\left(R_\rho\right) \cdot Ra^{1/3} k_T \tag{4}$$

$$C = 0.0032 \cdot \exp\left(4.8 \cdot R_\rho^{0.72}\right) \tag{5}$$

$$Ra = 0.25 \cdot 10^9 R_\rho^{-1.1} \tag{6}$$

$$K_S = R_\rho R_F K_T, \tag{7}$$

where k_T is the molecular diffusivity of heat; $R_F = R_P K_T / K_S$ is the vertical flux ratio.

[42] The rate of buoyancy exchange for both salt fingering and diffusive regimes can be written using equations (2)–(3) and (4)–(7) as:

$$K_\rho = \frac{R_\rho K_T + K_S}{R_\rho + 1} = \frac{R_F + 1}{R_\rho + 1} \cdot K_S. \tag{8}$$

Equation (8) defines K_ρ as a function of the density ratio, assuming a locally linear equation of state. A constant value $R_F = 0.7$ is used for the heat/salt buoyancy flux ratio due to salt fingers, and as a function of R_ρ for diffusive convection [*Kelly*, 1990]:

$$R_F = \frac{\alpha F_T}{\beta F_S} = \frac{1/R_\rho + 1.4 \cdot \left(1/R_\rho - 1\right)^{3/2}}{1 + 14 \cdot \left(1/R_\rho - 1\right)^{3/2}}. \tag{9}$$

[43] The vertical temperature and salinity gradients measured through the interface between the FSBW and the BSBW cores (360–410 m) are $-27.8\ 10^{-3}$ °C/m and $-19.4\ 10^{-4}$ psu/m, respectively (Figure 6). These values correspond to an $R_\rho \approx 1.39$, identifying the intensive salt-finger layering through the interface. The diffusivities for salt and heat computed using equations (4)–(7) are $7.0 \cdot 10^{-4}$ and $3.5\ 10^{-4}$ m^2/s, respectively. These estimations are an order of magnitude higher then estimations of diffusivities in a stable salt-fingering interface made by *Rudels et al.* [1999]. The difference can likely be attributed to the lower values of R_ρ (compare 1.39 with 1.8 used by *Rudels et al.* [1999]). The diffusivity of buoyancy (K_ρ) computed using equations (2)–(3) and (8) is about $-0.54 \cdot 10^{-4}$ m^2/s. The negative value for the density diffusion coefficient indicates that double-diffusive motions decrease the potential energy of the system, in contrast to turbulent mixing, which tends to increase the system's potential energy by dissipating kinetic energy. For the specific potential density gradient of $8.3\ 10^{-4}$ kg/m^4 this density diffusion coefficient implies a buoyancy flux of $-4.5\ 10^{-8}$ kg/s m^2 without background turbulence that is related to any process other than double-diffusive processes.

[44] The temperature and salinity vertical gradients through the lower boundary of the BSBW core (550–660 m) are $2.8\ 10^{-3}$ °C/m and $4.9\ 10^{-4}$ psu/m, respectively (Figure 6), resulting in a density ratio $R_\rho \approx 0.52$ that is also indicative of moderate-to-strong mixing of heat and salt induced by diffusive convection. Our estimates of the diffusivity for salt and heat are about $8.7 \cdot 10^{-7}$ and $7.1 \cdot 10^{-6}$ m^2/s, respectively. These heat diffusivities exceed those reported by *Padman and Dillon* [1989], and *Rudels et al.* [1999] by 4–7 times. The diffusivity of buoyancy computed using equations (4)–(8) is about $0.06 \cdot 10^{-4}$ m^2/s. For the specific vertical density gradient of $2.0\ 10^{-4}$ kg/m^4, this diffusivity of buoyancy implies a buoyancy flux of $-0.12\ 10^{-8}$ kg/s m^2. Like in the salt-finger interfaces, the negative diffusive-convection flux indicates an upward flux of buoyancy which decreases the potential energy of the water column.

[45] The buoyancy flux at the interface between the eddy FSBW and BSBW cores is an order of magnitude higher than below the BSBW core, as a result of both a higher vertical density gradient and a higher rate of heat and flux exchange through the salt-finger interface. Thus we can speculate that salt-fingering dominates diffusive convection and governs the evolution of temperature, salinity, and density within the BSBW eddy core.

[46] We roughly estimate the lifetime of an eddy as the time that is needed for the BSBW core characteristics to decay to the level of ambient waters, assuming this decay is affected only by the vertical diffusivity driven by salt fingering:

$$t_T = \frac{Q_T}{\rho C_P K_T T_z} \quad \text{and} \quad t_S = \frac{Q_S}{K_S S_z}, \tag{10a}$$

where Q_T and Q_S are heat and salt content differences, respectively, between the cold BSBW core and the ambient waters in the 380–650 m depth range; K_T and K_S are taken from equations (2)–(3), and T_z and S_z are vertical gradients of temperature and salinity through the interface between FSBW and BSBW cores. In fact, we specify the lifetime as the ratio of initial heat and salt contents of the BSBW core to the corresponding fluxes through the salt-finger interface.

[47] The quantities of $Q_T = 4.1\ 10^8$ J/m^2 and $Q_S = 11.1$ psu m in equation (10) imply a cold core lifetime of 1123 d for heat, and 937 d for salt anomalies. Furthermore, it seems that under this simplified definition the BSBW core lifetime is underestimated since vertical gradients of temperature and salinity tend to decrease with time. Using 2.4 cm/s as the AW boundary current velocity [*Dmitrenko et al.*, 2008; *Woodgate et al.*, 2007] yields a distance of 2000 km at which the eddy's thermohaline structure is still distinct from the ambient surrounding water. Thus assuming no additional mixing through interaction with the mean flow or/and steering over the rough topography, the measured eddy is a potential vehicle for heat and salt transport to the remote parts of the Nansen and even the Canada basins.

5.3. Evolution From the Source to the Mooring Site: Evidence From Numerical Simulation

[48] The quantitative assessment of the eddy present state in section 5.2 reveals that this state is mainly governed by double-diffusion. Numerical simulation provides an effective tool with which to explore double-diffusive instability. The two- or three-dimensional numerical models are usually employed to reproduce the main patterns of double-diffusive mixing (see, e.g., an overview by *Yoshida and Nagashima* [2003]). The longevity of the recorded isolated eddy makes it possible to simplify the governing equations to the one-dimensional. We will therefore employ a one-dimensional numerical model to simulate the evolution of temperature, salinity, and density vertical profiles through the eddy core along its translation path from the source area to the mooring position with the main purpose of studying the governing processes and identity between observed and simulated patterns.

[49] In section 5.1 we showed that the eddy retains the identity of its source water for a distance of about 1100 km downstream from the source location. This suggests that lateral mixing might not occur solely by diffusive processes. The suppressed lateral exchange implies that one-dimensional thermal and salt diffusion equations can be used to define the translation of eddy properties from the eddy source in the northern Kara Sea downstream to the mooring position as:

$$\frac{\partial \psi}{\partial t} = \frac{\partial}{\partial z} K_\psi \frac{\partial \psi}{\partial z}, \tag{10b}$$

where ψ indicates the tracer of temperature (T) or salinity (S).

[50] A numerical simulation of equation (10b) was initialized for conditions that roughly reproduce the vertical temperature and salinity distribution in the northern Kara Sea downstream from the confluence of the FSBW and the

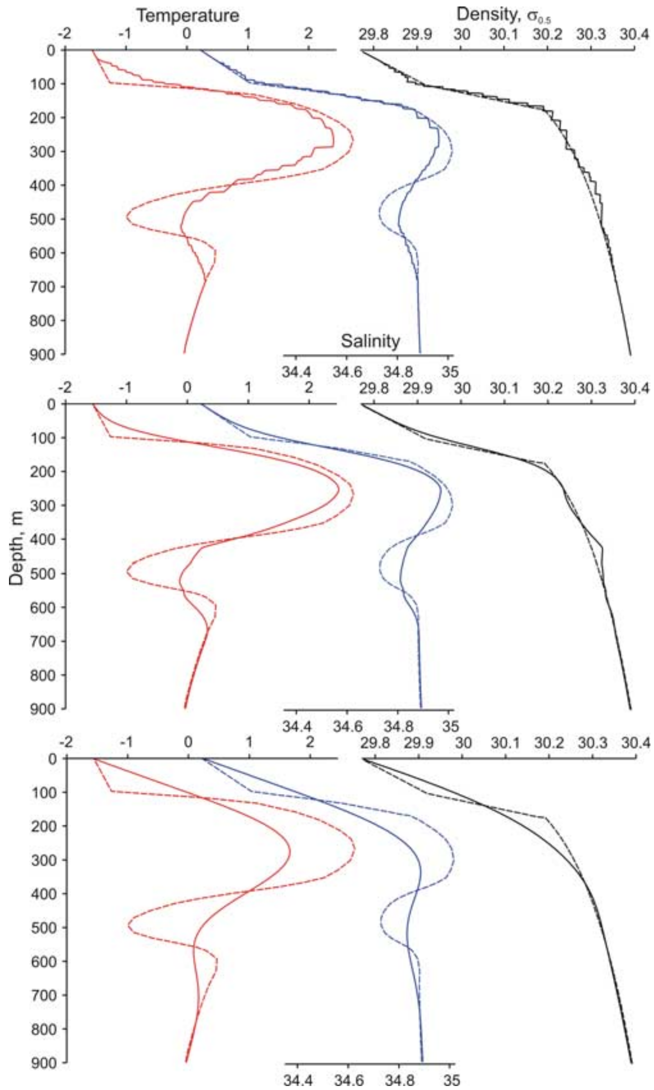

Figure 9. Numerically simulated evolution of temperature (red), salinity (blue), and potential density (black) vertical profiles forced by (top) double-diffusive mixing, (center) double-diffusive mixing with background turbulence diffusivity of 10^{-5} m^2/s, and (bottom) purely turbulent mixing with diffusivity of 10^{-4} m^2/s. Dashed lines demonstrate initial conditions; solid lines represent numerically modeled profiles after 24-month simulation.

BSBW (Figure 9). The FSBW core temperature and salinity were taken as 2.7°C and 35.00 psu at the core depth of 285 m. The BSBW core was defined to be deeper (500 m), with a temperature and salinity of −1°C and 34.73 psu, respectively. Zero fluxes of mass, heat, and salt were imposed at the top and bottom boundaries. The double-diffusion diapycnal eddy diffusivity was taken as in equations (2)–(7).

[51] Following *Muench et al.* [1990], background diffusivity is also included in the parameterization for double-diffusive processes by adding K_∞ to the right-hand parts of equations (2)–(4) and (7). Here K_∞ indicates mixing intensity that does not refer to the double diffusion. For stable conditions ($R_\rho < 0$), we use a vertically uniform background diapycnal mixing intensity for both temperature and salinity to represent mixing in double-stability:

$$K_\psi = K_\infty \tag{11}$$

.

[52] At each step of integration, a time constant Δt was defined as one-half of the Courant stability criterion:

$$\Delta t = \frac{\Delta z^2}{4K_{\max}}, \tag{12}$$

where Δz is vertical grid spacing (1 m), and $K_{\max}$ is a maximal temperature or salinity diffusivity over the entire water column at the current integration step. The simulation has been run for 24 months, approximately corresponding to the eddy traveltime from the northern Kara Sea to the mooring (about 1100 km) with velocity of 1.8 cm/s [*Frank et al.*, 1998; *Karcher et al.*, 2003]. Note that *Dmitrenko et al.* [2008] and *Woodgate et al.* [2001] estimate velocity from data downstream from the mooring site at 2.4 cm/s and 5 cm/s respectively based on current meters and TS advection.

[53] Three different scenarios were applied. The first simulates only the double-diffusive instability. The initial and 24-month simulated profiles of temperature, salinity, and density are shown in Figure 9 (top). Of particular interest is formation of the thermohaline staircases beginning from the initial continuously stratified profiles that are typical of double-diffusive convection. These patterns were also observed through the eddy center at the upper FSBW layer and at the lower part of the interface between the FSBW and BSBW eddy cores (Figure 6).

[54] In the second scenario the double-diffusive instability was accompanied by a background turbulent diffusivity of 10^{-5} m^2/s. One may conclude that using background turbulent diffusivity results in substantial degradation of the thermohaline staircases (Figure 9, center). Moreover, the simulated BSBW core, being neutrally stratified by density from 420 to 520 m, exhibits temperature and salinity stratification as shown in Figure 9 (center) that is consistent with the MMP observations through the eddy center in the upper layer of the BSBW eddy core between 425 m and 475 m (Figure 6). There is no substantial difference between the simulated upper and lower core temperatures and salinities for the first and second scenario.

[55] The third scenario simulates the evolution of vertical temperature, salinity, and density profiles due solely to a background turbulent diffusivity of 10^{-4} m^2/s (Figure 9, bottom). One may conclude that there are no thermohaline staircases attributed to the double-diffusion instability, and the simulated vertical profiles are smoother. The FSBW core temperature and salinity are substantially lower than in the first and second scenarios. Furthermore, the turbulent mixing nearly disrupts the BSBW core by tending to form a homogeneous mixed layer in the lower interface between the BSBW and the surrounding water. However, the density still remains continuously stratified.

[56] We argue that our simplified model does reveal the predominance of double-diffusive instability in the translation of an eddy from the northern Kara Sea to the central

Laptev Sea. While in our third numerical experiment the turbulent mixing completely disrupts thermohaline staircases (Figure 9, bottom), the observational record clearly demonstrates their occurrence through the interface between the FSBW and the BSBW as well as in the FSBW upper layer (Figure 6). This conclusion also agrees with our estimation of the gradient Richardson number in Figure 8 (right) which detects no occurrence of shear instability (Ri < 0.25) anywhere in the eddy.

[57] It is not surprising that the simulated pattern from our numerical simulation did not identically reproduce the observed patterns. The zero fluxes at the upper and lower boundaries and stationary, vertically uniform background turbulent diffusivity are likely among the potential reasons. These simplifications result in several contradictions between simulation and observations. The simulated shear instability is assumed to be mainly responsible for local mixing observed in the lower layer of the BSBW core deeper than 500 m (compare Figure 9, bottom and Figure 6). The disappearance of the thermohaline staircases at the lower interface of the BSBW core also supports this speculation. At the same time, the shear instability disrupts the double-diffusive staircases measured through the FSBW core interface at 150–250 m and 350–450 m and reproduced by our first numerical experiment with double-diffusive instability (compare Figure 9, top and bottom, and Figure 6). It seems more likely that the turbulent background diffusivity of 10^{-5} m^2/s was overestimated in the second experiment with respect to the upper eddy layer, and underestimated in the lower eddy layer. Our estimations of system susceptibility to shear instability in Figure 8 (right) corroborate this conclusion.

[58] Our experiments clearly confirm the weak rate of lateral exchange through the eddy interfaces and its importance for the mean AW flow. The cooling in the FSBW core that occurs during eddy translation from the Kara to the Laptev Sea is explained well by the simulated double-diffusive vertical mixing without lateral exchange. The provisional FSBW cooling varies within a range of 0.1–0.5°C depending on initial conditions in the northern Kara Sea. Cooling simulated in the first and second numerical experiments was 0.3°C. At the same time, the ambient FSBW core cooling is estimated to be 1.2–1.6°C. The BSBW core warming exhibits similar patterns in observational and simulated data (Figure 6 and Figure 9, top and center). Moreover, the turbulent diffusivity of 10^{-4} m^2/s in the third experiment results in overestimation of the FSBW cooling (compare the FSBW core temperature of 2.5°C and 1.7°C for the second and third experiments, respectively; Figure 9, center and bottom). The simulated BSBW core temperature varies from −0.2°C to 0.1°C for the second and third experiments respectively; the simulated value from the third experiment is identical to the measured value of 0.1°C (Figure 6 and Figure 9, center and bottom).

[59] We conclude that our results demonstrate the predominance of double-diffusion instability in convective modification of the upper eddy layer down to the BSBW core with a background turbulent diffusivity of less than 10^{-5} m^2/s. The lower layer modification seems to be governed by shear instability with a turbulent diffusivity of about 10^{-4} m^2/s. Our quantitative assessment given in section 5.2 is consistent with these results. Furthermore, the thermohaline staircases evident in the MMP record for the FSBW interfaces and completely absent in the BSBW lower interface (Figure 6) also support our conclusions. The discrepancy between observed and numerically simulated density evolution is most likely attributable to the zero buoyancy fluxes through the vertical eddy boundaries. While the lateral exchange through the eddy interfaces is relatively weak, at upper and lower eddy boundaries it may become more important, providing the valuable lateral buoyancy fluxes that are not properly described by our simplified model.

6. Summary and Concluding Remarks

[60] An eddy, observed in February 2005 approximately 1100 km from its supposed formation site, had a thickness of at least 650 m, and was composed of two distinct, vertically aligned cores. The upper core was warmer (2.6°C), saltier (34.88 psu), stably stratified vertically, and with density not substantially different from the ambient. The lower core was cooler (0.1°C), fresher (34.81 psu), neutrally vertically stratified, and lighter than surrounding ambient water by 0.02 kg/m^3. The eddy was rather homogeneous out to a radius of at least 3.4 km, with a radius of maximum velocity of 14.5 km, and an entire diameter of about 27 km or greater. We hypothesize that this eddy is generated in the northern Kara Sea from the instabilities of the front separating two different branches of the AW inflow to the Arctic Ocean. The upper core consists of AW entering the Arctic Ocean through Fram Strait, and the lower core is attributed to the AW inflow through the Barents and northern Kara seas.

[61] Assessment of the thermohaline conditions through the eddy reveals that salt-fingering dominates diffusive convection and governs the evolution of temperature, salinity, and density throughout the eddy. Through the interface between the upper and lower cores the salt fingering instability results in a buoyancy diffusivity of about 0.54 10^{-4} m^2/s. The buoyancy diffusivity through the lower core originating from diffusive instability is about 10 times lower (0.06 10^{-4} m^2/s). While there is no evidence of shear instability based on the usual R_i < 0.25 criterion, shear instability may be suspected through the eddy cores and the water underlying the BSBW core. Projecting our assessment downstream from the time of eddy formation, we found that the eddy is able to translate its thermohaline anomaly several thousand kilometers downstream from its source location.

[62] Numerical modeling using one-dimensional thermal and salt diffusion equations was applied to examine the processes governing the evolution of eddy thermohaline properties downstream from the hypothesized source area. The eddy retains the identity of its source water for a distance of about 1100 km downstream from the hypothesized source location. This identity stability suggests that lateral mixing might not occur solely by diffusive processes and implies the accuracy of the one-dimensional assumption that we used for numerical simulation of eddy modification. Despite uncertainties in determining the initial conditions and oversimplified boundary conditions, the computed temperature and salinity profiles exhibit similarities to measured data, providing evidence that the modification

of the upper eddy layer is mostly dominated by double-diffusive convection with a background turbulent diffusivity of less than 10^{-5} m^2/s. Modification of the lower eddy layer seems to be dominated by shear instability with a turbulent diffusivity of about 10^{-4} m^2/s. The distinct difference between eddy thermohaline properties and the properties of the surrounding AW layer invites speculation that along-slope modification of the ambient AW topographically steered boundary current (the FSBW cooling and the BSBW warming) is likely dominated by lateral processes, while the diffusivity through the eddy is much smaller and is mainly attributable to vertical fluxes. This speculation is consistent with the proposition by *Carmack et al.* [1997] about the importance of littoral fluxes in facilitating the property transport from the continental margins into the interior ocean.

[63] There are also some caveats to our analysis. We assume that the FSBW and the BSBW in the northern Kara Sea interact isopycnically, but diapycnal interactions driven by less-well-known external forces may also occur. The BSBW core might be mixed due to steering over rough bottom topography before and/or after confluence with the FSBW. Our modeling results do not provide an acceptable interpretation of the lower eddy core's diapycnicity relative to surrounding ambient water. The model presented is one-dimensional and does not address the possibility of lateral motions. The instabilities that can lead to eddy formation imply lateral shear; hence, advection and the accompanying possibility of lateral exchanges (which was not part of our analysis) may explain those components of the observed thermohaline patterns that are not well described by our simplified one-dimensional model. The discrepancy between observed and simulated vertical density distribution requires further investigation.

[64] **Acknowledgments.** I.D. and V.I. thank the NOAA-funded IARC Program "Nansen and Amundsen Basins Observational System" (NABOS) for financial support. S.K. acknowledges funding through the NAVO grant N00014-04-1-0775. I.D. and S.K. also appreciate the financial support through the BMBF project "System Laptev Sea" (03G0639A). Additional support was provided by the Frontier Research System for Global Change (V.I. and S.K.). The authors gratefully acknowledge G. C. Johnson for providing MATLAB code for the MMP conductivity thermal mass error correction. We gratefully acknowledge Ursula Schauer for CTD profiles taken in 1993–1996 from the RV Polarstern. We are grateful to Robin Muench and two other anonymous reviewers for constructive comments and criticism.

References

Aagaard, K. (1989), A synthesis of the Arctic Ocean circulation, *ICES Mar. Sci. Symp.*, *188*, 11–22.

Abarbanel, H. D., D. D. Holm, J. E. Marsden, and T. Ratiu (1984), Richardson number criterion for the nonlinear stability of three-dimensional stratified flow, *Phys. Rev. Lett.*, *52*, 2352–2355.

Carmack, E., R. Macdonald, R. Perkin, F. McLaughlin, and R. Pearson (1995), Evidence for warming of Atlantic water in the southern Canadian Basin of the Arctic Ocean: Evidence from the Larsen-93 Expedition, *Geophys. Res. Lett.*, *22*(9), 1061–1065.

Carmack, E. C., K. Aagaard, J. H. Swift, R. W. MacDonald, F. A. McLaughlin, E. P. Jones, R. G. Perkin, J. N. Smith, K. M. Ellis, and L. R. Killius (1997), Changes in temperature and tracer distributions within the Arctic Ocean: Results from the 1994 Arctic Ocean section, *Deep Sea Res. II*, *44*(8), 1487–1502.

D'Asaro, E. A. (1988), Observations of small eddies in the Beaufort Sea, *J. Geophys. Res.*, *93*(C6), 6669–6684.

Dmitrenko, I. A., I. V. Polyakov, S. A. Kirillov, L. A. Timokhov, H. L. Simmons, V. V. Ivanov, and D. Walsh (2006), Seasonal variability of Atlantic water on the continental slope of the Laptev Sea during 2002–2004, *Earth Planet. Sci. Lett.*, *244*(3–4), 735–743, doi:10.1016/j.epsl.2006.01.067.

Dmitrenko, I. A., I. V. Polyakov, S. A. Kirillov, L. A. Timokhov, I. E. Frolov, V. T. Sokolov, H. L. Simmons, V. V. Ivanov, and D. Walsh (2008), Towards a warmer Arctic Ocean: Spreading of the early 21st century Atlantic water warmer anomaly along the Eurasian Basin margins, *J. Geophys. Res.*, *113*, C05023, doi:10.1029/2007JC004158.

Foreman, M. G. G. (1977), Manual for tidal heights analysis and prediction, *Pacific Marine Science Report*, *77–10*, Inst. of Ocean Sci., Patricia Bay, Sidney, B.C., 58 pp.

Frank, M., W. M. Smethie, and R. Bayer (1998), Investigation of subsurface water flow along the continental margin of the Eurasian Basin using the transient tracers tritium, ^{3}He, and CFCs, *J. Geophys. Res.*, *103*(C13), 30,773–30,792.

Hanzlick, D., and K. Aagaard (1980), Freshwater and Atlantic water in the Kara Sea, *J. Geophys. Res.*, *85*(C9), 4937–4942.

Howard, L. N. (1961), Note on a paper of John Miles, *W. J. Fluid Mech.*, *10*, 509.

Johnson, G. C., J. M. Toole, and N. G. Larson (2007), Sensor corrections for Sea-Bird SBE-41CP and SBE-41 CTDs, *J. Atmos. Oceanic Technol.*, *24*, 1117–1130.

Karcher, M. J., R. Gerdes, F. Kauker, and C. Koberle (2003), Arctic warming: Evolution and spreading of the 1990s warm event in the Nordic seas and the Arctic Ocean, *J. Geophys. Res.*, *108*(C2), 3034, doi:10.1029/2001JC001265.

Kelley, D. E. (1984), Effective diffusivities within oceanic thermohaline staircases, *J. Geophys. Res.*, *89*(C6), 10,484–10,488.

Kelley, D. E. (1990), Fluxes through diffusive staircases: A new formulation, *J. Geophys. Res.*, *95*(C3), 3365–3371.

Kostianoy, A. G., and I. M. Belkin (1989), A survey of observations on intrathermocline eddies in the world ocean, in *Mesoscale/Synoptic Coherent Structures in Geophysical Turbulence: Proceedings of the 20th International Liège Colloquium on Ocean Hydrodynamics*, edited by J. C. J. Nihoul and B. M. Jamart, *Elsevier Oceanogr. Ser.*, *50*, 821–841.

Manley, T. O., and K. Hunkins (1985), Mesoscale eddies of the Arctic Ocean, *J. Geophys. Res.*, *90*(C3), 4911–4930.

McLaughlin, F. A., E. C. Carmack, R. W. Macdonald, A. Weaver, and J. N. Smith (2002), The Canada Basin 1989–1995: Upstream events and far-field effects of the Barents Sea, *J. Geophys. Res.*, *107*(C7), 3082, doi:10.1029/2001JC000904.

McWilliams, J. C. (1985), Submesoscale coherent vortices in the ocean, *Rev. Geophys.*, *23*(2), 165–182.

Merryfield, W. (2002), Intrusions in double-diffusively stable Arctic waters: Evidence for differential mixing?, *J. Phys. Oceanogr.*, *32*, 1452–1459.

Miles, J. W. (1961), On the stability of heterogeneous shear flow, *J. Fluid Mech.*, *10*, 496–508.

Miles, J. W. (1963), On the stability of heterogeneous shear flows. Part 2, *J. Fluid Mech.*, *16*, 209–227.

Miles, J. W. (1986), Richardson's criterion for the stability of stratified shear flow, *Phys. Fluids*, *29*, 3470–3471.

Muench, R. D., H. J. S. Fernando, and G. R. Stegen (1990), Temperature and salinity staircases in the northwestern Weddell Sea, *J. Phys. Oceanogr.*, *20*, 295–306.

Muench, R. D., J. T. Gunn, T. E. Whitledge, P. Schlosser, and W. E. Smethie (2000), An Arctic Ocean cold core eddy, *J. Geophys. Res.*, *105*(C10), 23,997–24,006.

Newton, J. L., K. Aagaard, and L. K. Coachman (1974), Baroclinic eddies in the Arctic Ocean, *Deep Sea Res., Part I or Part II*, *21*, 707–719.

Padman, L., and T. M. Dillon (1989), Thermal microstructure and internal waves in the Canadian Basin diffusive staircase, *Deep Sea Res., Part I or Part II*, *36*, 531–542.

Polyakov, I., D. Walsh, I. Dmitrenko, R. L. Colony, and L. A. Timokhov (2003), Arctic Ocean variability derived from historical observations, *Geophys. Res. Lett.*, *30*(6), 1298, doi:10.1029/2002GL016441.

Polyakov, I. V., G. V. Alekseev, L. A. Timokhov, U. S. Bhatt, R. L. Colony, H. L. Simmons, D. Walsh, J. E. Walsh, and V. F. Zakharov (2004), Variability of the intermediate Atlantic water of the Arctic Ocean over the last 100 years, *J. Clim.*, *17*(23), 4485–4497.

Polyakov, I., et al. (2005), One more step toward a warmer Arctic, *Geophys. Res. Lett.*, *32*, L17605, doi:10.1029/2005GL023740.

Polzin, K. L. (1996), Statistics of the Richardson number: Mixing models and fine structure, *J. Phys. Oceanogr.*, *26*(8), 1409–1425.

Prater, M. D., and T. B. Sanford (1994), An eddy off Cape St. Vincent. part I: Description, *J. Phys. Oceanogr.*, *24*(7), 1572–1586.

Quadfasel, D., A. Sy, D. Wells, and A. Tunik (1991), Warming in the Arctic, *Nature*, *350*, 385.

Rozhkova, A.Yu., I. A. Dmitrenko, D. Bauch, and L. A. Timokhov (2008), Variations in characteristics of the Barents branch of the Atlantic Water in the Nansen Basin under the influence of atmospheric circulation over the

Barents Sea, *Dokl. Acad. Sci. USSR, Earth Sci. Ser., Engl. Transl.*, *418*(3), 149–154.

Ruddick, B. (1983), Note: A practical indicator of the stability of the water column to double-diffusive activity, *Deep Sea Res., Part A*, *30*, 1105–1107.

Rudels, B., G. Bjork, R. D. Muench, and U. Schauer (1999), Double-diffusive layering in the Eurasian Basin of the Arctic Ocean, *J. Mar. Syst.*, *21*, 3–27.

Rudels, B., R. Meyer, E. Fahrbach, V. Ivanov, S. Osterhus, D. Quadfasel, U. Schauer, V. Tverberg, and R. A. Woodgate (2000), Water mass distribution in Fram Strait and Yermak Plateau in summer 1997, *Ann. Geophys.*, *18*, 687–705.

Schauer, U. E., R. D. Muench, B. Rudels, and L. Timokhov (1997), Impact of eastern Arctic shelf waters on the Nansen Basin intermediate layers, *J. Geophys. Res.*, *102*(C2), 3371–3382.

Schauer, U., H. Loeng, B. Rudels, V. K. Ozhigin, and W. Dieck (2002a), Atlantic Water flow through the Barents and Kara Seas, *Deep Sea Res., Part I*, *49*(12), 2281–2298, doi:10.1016/S0967-0637(02)00125-5.

Schauer, U., B. Rudels, E. P. Jones, L. G. Anderson, R. D. Muench, G. Björk, J. H. Swift, V. Ivanov, and A. M. Larsson (2002b), Confluence and redistribution of Atlantic water in the Nansen, Amundsen and Makarov basins, *Ann. Geophys.*, *20*(2), 257–273.

Schauer, U., E. Fahrbach, S. Osterhus, and G. Rohardt (2004), Arctic warming through the Fram Strait - Oceanic heat transport from three years of measurements, *J. Geophys. Res.*, *109*, C06026, doi:10.1029/2003JC001823.

Schmitt, R. W. (1981), Form of temperature–salinity relationship in the central water: Evidence for double-diffusive mixing, *J. Phys. Oceanogr.*, *11*, 1015–1026.

Schmitt, R. W. (1988), Mixing in a thermohaline staircase, in *Small-Scale Turbulence and Mixing in the Ocean*, vol. 46, edited by J. Nihoul and B. Jamart, pp. 435–452, *Elsevier Oceanogr. Ser.*, Elsevier, New York.

Schmitt, R. W., J. R. Ledwell, E. T. Montgomery, K. L. Polzin, and J. M. Toole (2005), Enhanced diapycnal mixing by salt fingers in the thermocline of the tropical Atlantic, *Science*, *308*, 685–688.

Timofeev, V. T. (1957), Atlantic waters in the Arctic Basin (in Russian), *Probl. Arkt.*, *2*, 41–52.

Turner, J. S. (1973), *Buoyancy Effects in Fluids*, 367 pp., Cambridge Univ. Press, New York.

Woodgate, R. A., K. Aagaard, R. D. Muench, J. Gunn, G. Bjork, B. Rudels, A. T. Roach, and U. Schauer (2001), The Arctic Ocean boundary current along the Eurasian slope and the adjacent Lomonosov Ridge: Water mass properties, transports and transformations from moored instruments, *Deep Sea Res., Part I*, *48*, 1757–1792.

Woodgate, R. A., K. Aagaard, J. H. Swift, W. M. Smethie Jr., and K. K. Falkner (2007), Atlantic water circulation over the Mendeleev Ridge and Chukchi Borderland from thermohaline intrusions and water mass properties, *J. Geophys. Res.*, *112*, C02005, doi:10.1029/2005JC003416.

Yoshida, J., and H. Nagashima (2003), Numerical experiments on salt-finger convection, *Prog. Oceanogr.*, *56*, 435–459.

Zhang, J., R. W. Schmitt, and R. X. Huang (1998), Sensitivity of the GFDL modular ocean model to parameterization of double-diffusive processes, *J. Phys. Oceanogr.*, *28*, 589–605.

I. A. Dmitrenko, Department of Paleoceanography, Leibniz Institute of Marine Sciences, University of Kiel, Building 4, Wischhofstrasse 1-3, Kiel, D-24148, Germany. (idmitrenko@ifm-geomar.de)

V. V. Ivanov, International Arctic Research Center, University of Alaska Fairbanks, 930 Koyukuk Drive, Fairbanks, AK 99775-7340, USA. (vivanov@iarc.uaf.edu)

S. A. Kirillov, Department of Oceanology, Arctic and Antarctic Research Institute, 38 Bering Street, St. Petersburg, 199397, Russia. (dia@aari.nw.ru)

R. A. Woodgate, Polar Science Center, Applied Physics Laboratory, University of Washington, 1013 NE 40th Street, Seattle, WA 98105-6698, USA. (woodgate@apl.washington.edu)